Chemical Engineering Journal xxx (xxxx) xxx–xxx

Contents lists available at ScienceDirect

Chemical Engineering Journal

journal homepage: www.elsevier.com/locate/cej

CO temperature-programmed desorption of a hexameric copper hydride nanocluster catalyst supported on functionalized MWCNTs for active site characterization in a low-temperature water–gas shift reaction

Luqmanulhakim Baharudin[a], Alex C.K. Yip[a], Vladimir B. Golovko[b], Matthew I.J. Polson[b], Matthew J. Watson[a,*]

[a] Department of Chemical and Process Engineering, College of Engineering, University of Canterbury, Private Bag 4800, Christchurch 8140, New Zealand
[b] School of Physical and Chemical Sciences, College of Science, University of Canterbury, Private Bag 4800, Christchurch 8140, New Zealand

HIGHLIGHTS

- Crystal structure complex of $[(PPh_3)CuH]_6$·0.75THF was determined.
- Cu_6 nanoclusters precursor changed phase to Cu_2O as active phase for LTWGS.
- Cu_2O is active on its most dominant facets (1 1 0), (1 1 1), (2 0 0) and (2 2 0).
- 1 wt% Cu_6 on functionalized MWCNTs exhibited optimal hypothetical activity.
- Operating temperature range is governed by water dew point and Cu sintering.

GRAPHICAL ABSTRACT

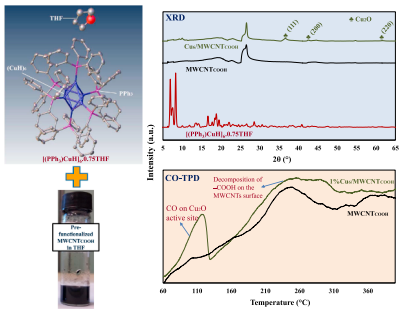

ARTICLE INFO

Keywords:
Active site characterization
Copper nanoclusters
CO chemisorption
CO temperature-programmed desorption
Multi-walled carbon nanotubes
Water-gas shift

ABSTRACT

A family of novel catalysts was generated using chemically synthesised, atomically precise hexameric copper hydride nanoclusters (Cu_6) deposited on carboxyl-pre-functionalized multi-walled carbon nanotubes ($MWCNT_{COOH}$). The $Cu_6/MWCNT_{COOH}$ catalysts were synthesized by wet impregnation of $MWCNT_{COOH}$ with varying copper loading contents (0.5–15 wt%). The study of the interaction between active sites in these materials with CO at low temperatures using CO temperature-programmed desorption in conjunction with the elementary steps in the Langmuir-Hinshelwood mechanism of low-temperature water–gas shift (LTWGS) reaction allowed us to predict the potential catalytic performance of the synthesized catalysts in the LTWGS. The hypothetical activities were correlated with the catalyst surface characterization by CO chemisorption (Cu dispersion, crystallite size and surface area) and characterization of the active phase composition by XRD, showing good agreement. Optimal copper loading was identified to be 1 wt% based on the highest Cu surface area per sample weight and dispersion, and the amount of CO adsorbed per sample weight. The predicted catalytic performance was analysed as a function of support type: $MWCNT_{COOH}$ *cf.* non-functionalized MWCNTs and alumina with fixed Cu loading of 1 wt%. The CO reactivity was analysed on Cu_2O crystallites as the active phase, with a focus on the most dominant facets: (1 1 0), (1 1 1), (2 0 0) and (2 2 0). A comparison was made with a sample consisting of Cu nanoparticles (Cu_{NP}) supported on $MWCNT_{COOH}$, and a reference commercial catalyst, 51%CuO/31%ZnO-Al_2O_3.

* Corresponding author.
E-mail address: matthew.watson@canterbury.ac.nz (M.J. Watson).

https://doi.org/10.1016/j.cej.2018.10.215

It is expected that the optimal catalyst, 1%Cu_6/$MWCNT_{COOH}$, is active for LTWGS reaction from temperatures as low as 120 °C (governed by dew point of water) up to temperatures well below industrial operating temperatures (constrained by temperature rise due to the exothermic reaction that leads to Cu_6 sintering).

1. Introduction

The water–gas shift (WGS) reaction is an industrially important reaction that often follows steam reforming of hydrocarbons in a typical hydrogen production plant [1,2]. The reaction is generally favoured for not only hydrogen enrichment but also the removal of CO for high-purity hydrogen production, in which the remaining ~10 v/v% CO [3,4] content in the synthesis gas of the reformer outlet is further converted to carbon dioxide and additional hydrogen by a reaction with steam [5,6], reducing the concentration of CO to ~0.5–1 v/v% [3]. The hydrogen produced by the reforming reaction and the shift conversion is typically used in ammonia synthesis in the fertilizer industry, in a petroleum refinery for various processes, such as hydrodesulphurisation, and as a fuel in hydrogen-fuelled vehicles and for power generation [1,5,7,8].

The water–gas shift reaction is a reversible reaction that can be expressed by Eq. (1) [1–5,7,9]:

$$CO + H_2O \leftrightarrow CO_2 + H_2 \quad \Delta H_{298}{}^0 = -41.09\ \text{kJ/mol} \tag{1}$$

The reaction is moderately exothermic, and the conversions are limited by chemical equilibrium. For an exothermic reaction, the equilibrium constant is higher at a lower operating temperature, thermodynamically favouring higher equilibrium CO conversion. However, under such low temperature conditions, the reaction is kinetically limited, *e.g.*, the reaction rate is lower [1,4,5,7,10]. The conversions are not affected by the variation of the operating pressure, but the higher concentrations of the reaction products, hydrogen and carbon dioxide, inhibit the rate of the forward reaction [10].

The industrially implemented WGS reaction during early days was operated in a single adiabatic reactor that produced a product mixture with residual CO content between 2 and 4% as equilibrium was approached. The temperature along the reactor length increased as a result of the exothermic reaction, inhibiting further CO conversion. To achieve the highest possible CO conversion and yet maintain a reasonably high rate of reaction for high-purity hydrogen production, lower operating temperatures are required. However, the iron oxide-chromium oxide catalysts commercially used in the reaction were kinetically limited under such conditions and could only be active at high temperatures. Therefore, the scheme has evolved to an array of multi-stage adiabatic reactors arranged in series, with a two-stage adiabatic reactor arrangement known as the high-temperature water–gas shift (HTWGS) followed by the low-temperature water gas shift (LTWGS) reactors becoming the most common. Such an arrangement required inter-bed cooling for removal of heat after HTWGS to maintain the inlet temperature of the LTWGS reactor together with the development of copper-based catalysts that are active at a low temperatures and capable of achieving sub-1% exit concentration of CO. The catalysts based on iron oxide structurally promoted with chromium oxide remain in use in the HTWGS reaction [1,5–7,10,11].

The iron-chromium-based catalyst bed in the HTWGS reactor is operated typically at reaction temperatures of 310–500 °C, reducing the outlet CO to concentrations that vary between 1% and 5%, depending on the feed gas compositions and exit temperature [1,5,7,10]. This is followed by operating the copper-based catalyst bed in the LTWGS reactor at operating temperatures of 190–250 °C [1,5], converting the residual CO further down to a sub-1% concentration at the reactor outlet [1,3,7,10].

Commercially available LTWGS catalysts can be found in the form of a mixture of ZnO, CuO and Cr_2O_3/Al_2O_3, in which the compositions and characteristics vary from one vendor to another [5,7,12]. Most catalyst development initiatives have been focused on the objective of achieving higher conversions of CO that can approach the equilibrium limit (Appendix A) more closely at low temperatures than those obtained on the commercial catalysts [3,10].

Due to equilibrium-limited CO conversions, research has been focused on the higher-activity catalysts [2,3,5] that are capable of improving the reaction rates at the thermodynamically favourable low-temperature operation regime of the exothermic LTWGS reaction. Whilst the Cu-ZnO catalysts are active in the temperature range of 190–250 °C, their low kinetic activity calls for the use of low gas hourly space velocity (GHSV) of 3,000–5,000 hr^{-1} [1,10]. An increased catalytic activity in the LTWGS reaction could lead to an increase in GHSV, reducing the catalyst volume in the adiabatic bed and thus saving operational and capital costs.

This paper presents a study that aims to demonstrate the characterization and catalytic activity features of a novel Cu_6/$MWCNT_{COOH}$ catalyst that is potentially suitable for ultra-low temperature WGS. In general, MWCNTs possess favourable surface textural properties with potential for further chemical modification of the surface for good metal particle dispersion. They possess a large surface area of 100–200 m^2/g [13] and have low tortuosity and high meso- and macroporosity while containing no micropores [13–16]. They also have a high specific pore volume in the range from 0.5 to 2 cm^3/g [14]. These properties maximize the effective diffusion coefficient [14] and minimize the internal mass transfer limitations within the thin filamentous layers [16], hence making them a good catalyst support for the reactant/product diffusion to/from the catalytic active sites in heterogeneous reactions. Furthermore, they have excellent heat transfer capabilities, which could become critical for the removal of heat generated by the exothermic WGS reaction from the catalyst bed [17].

In this work, the copper nanocluster-based catalysts were optimized by varying the Cu loading content. We aimed to predict the optimal Cu loading by comparing materials with Cu contents across a wide range of loading (0.5, 1, 5, 11, 13 and 15 wt%). CO chemisorption and XRD techniques were employed to measure the Cu dispersion, crystallite size and surface area and to characterize the surface chemistry and phase composition of the synthesized catalysts. The surface chemistry and phase composition characteristics of obtained materials were interpreted in light of the proposed active site properties to predict their performance in the LTWGS reaction. The activity predicted based on CO-TPD data was correlated with the analysis based on the established Langmuir-Hinshelwood (L-H) mechanism to provide a means to better screen and predict the activity of the catalyst in the LTWGS reaction.

Furthermore, we also investigated the effect of supports by comparing functionalized MWCNTs ($MWCNT_{COOH}$) with pristine MWCNTs and alumina as supports for the predicted optimal (1 wt%) loading with an aim to study the interaction of copper clusters with the novel MWCNT supports and the support commonly used in industry. Finally, a benchmark catalyst made using Cu nanoparticles deposited on functionalized MWCNTs at 1 wt% loading was studied to examine the effect of different pre-synthesised nanostructured Cu precursors (nanoclusters *vs.* nanoparticles). A commercial catalyst, 51%CuO/31%ZnO-Al_2O_3, was used as a reference.

2. Experimental

Pre-functionalized multi-walled carbon nanotubes (MWCNTs) grafted with carboxyl groups ($MWCNT_{COOH}$) on their wall surface

(99.9% purity, OD = 10–20 nm, length = 10–30 μm, specific surface area (SSA) = > 100 m^2/g, Nanostructured and Amorphous Materials Inc., USA), pristine MWCNTs (95 + % purity, OD = 10–20 nm, length = 0.5–2.0 μm, SSA = > 200 m^2/g, Nanostructured and Amorphous Materials Inc., USA) and alumina (Al_2O_3) (≥ 99%, SSA = 2.95 m^2/g, Sigma-Aldrich) were used as-purchased as the catalyst supports in this work. A commercial catalyst, 51%CuO/31%ZnO-Al_2O_3 (undisclosed vendor), was used for benchmarking and comparison purposes. The as-received mini-pellet-shaped commercial catalyst was first crushed into powder before use.

2.1. Sample preparation

2.1.1. Fabrication of Cu_6 cluster-based catalysts

The synthesis of Cu_6 nanoclusters was performed following the procedure described by Albert et al. (1989) [18] (Appendix A). To crystallize the $[(PPh_3)CuH]_6$ nanoclusters, the procedure described by Cook et al. (2016) [19] (Appendix A) was employed. Catalyst fabrication was performed using Schlenk-line technique. Weighing of Cu_6 clusters was performed in air as quickly as possible to minimize decomposition of these species, with a known mass of cluster (3.20 g) quickly transferred into a Schlenk tube with 50 mL of THF under Ar immediately after weighing to produce a stock solution with known concentration of cluster. On the basis of a total catalyst weight of 2.0 g, an amount of 1.98 g of pre-functionalized multi-walled carbon nanotubes (MWCNTs) grafted with carboxyl groups (–COOH) on their wall surface was vacuum-dried at 200 °C for 5 h to remove the traces of moisture as the support preparation step. The sample was then dispersed in tetrahydrofuran ($(CH_2)_4O$ = THF) solution under an argon atmosphere. An appropriate volume (10 mL) of the Cu_6 stock solution prepared in THF containing 0.02 g of copper (basis: Cu_6 nanoclusters empirical formula of $[(PPh_3)CuH]_6$·0.75THF) was added to the dispersed MWCNT suspension *via* a syringe. The wet impregnation was carried out by stirring the mixture at 750 rpm and room temperature overnight. After impregnation, the catalyst sample was vacuum-dried, and the flask containing the sample was then placed in a warm water bath (50 °C) for the last 10 min of the vacuum-drying step to remove residual solvent. The catalyst sample is denoted 1%Cu_6/$MWCNT_{COOH}$. The Cu_6 loading content was varied at 0.5, 5, 11, 13 and 15 wt% for a comparative analysis of the effect of loading on the catalytic activity. The same protocol was followed in the synthesis of 1%Cu_6 supported on pristine MWCNTs and alumina. The samples are denoted as 1%Cu_6/pristine MWCNT and 1%Cu_6/Al_2O_3, respectively. The samples were stored in air after their fabrication.

2.1.2. Fabrication of Cu nanoparticle-based catalyst

On the basis of a total weight of catalyst of 2 g, 1.98 g of $MWCNT_{COOH}$ was dispersed and stirred in methanol (UN 1230, CAS 67-56-1, Burdick & Jackson (B&J Brand ®)). A stock solution of copper chloride was prepared by dissolving 0.54 g of $CuCl_2{\cdot}2H_2O$ (Riedel-De Haën AG, Seelze-Hannover) (containing 0.2 g Cu) in 10 mL of methanol. An amount of 1.0 mL of the stock copper chloride solution (containing 0.02 g Cu) was pipetted into the dispersed $MWCNT_{COOH}$ support for copper loading of 1 wt%. The wet impregnation was carried out by stirring the mixtures overnight at 750 rpm and room temperature. The methanol dispersing the copper impregnated MWCNT sample was then removed under vacuum. The dry catalyst samples were then calcined in a nitrogen flow of 100 mL/min at 400 °C in a tubular furnace for 3 h, at a ramping rate of 2.5 °C/min. The catalyst sample is denoted as 1%Cu_{NP}/$MWCNT_{COOH}$, with the subscript NP referring to the nanoparticles.

2.2. Sample characterization

2.2.1. Phase composition

The powder diffraction patterns of the MWCNTs supports, pure micro-crystalline powder of crystallized $[(PPh_3)CuH]_6$, synthesized catalysts (as-prepared) and commercial catalyst (as-received) were recorded on an X-ray diffractometer (SuperNova, Agilent Technologies) over the 2θ range of 10–90°, using Cu-Kα radiation (λ = 0.154056 Å) operated at room temperature. The crystal structure and components of the nanoclusters were validated using the same X-ray diffractometer on a single-crystal form of the Cu_6 nanoclusters at 120 K.

2.2.2. Thermal stability

Both MWCNT support samples were analysed by thermogravimetric analysis (TGA) (SDT Q600, Alphatec Systems Ltd. supported by TA Instruments Universal Analysis 2000 software) under nitrogen flow of 100 mL/min, at a ramping rate of 50 °C/min, from an ambient condition up to 1200 °C to investigate their thermal stability under inert atmosphere. For the crystallized $[(PPh_3)CuH]_6$, the ramping rate used was 10 °C/min up to 400 °C.

2.2.3. Negative surface charge

The zeta potential of the MWCNT samples dispersed in deionized (DI) water was measured using Zetasizer Nano Series (Malvern Instruments Ltd., UK) at room temperature. The results were averaged, with each sample measurement repeated at least 4 times.

2.2.4. Dispersion/sedimentation

An amount of 0.050 g of pre-functionalized $MWCNT_{COOH}$ sample was centrifuged (MULTIFUGE 3 L, Heraeus) in 25 mL of DI water at 10,000 rpm for 20 min, and the parameters were halved for the same amount of pristine MWCNT sample in the same amount of DI water. The assessment was performed at room temperature.

2.2.5. Copper content

An amount of 0.050 g of each of the synthesized catalyst samples was digested in 2 mL *aqua regia* at 80 °C for 2 days (Appendix A) to dissolve the copper particles from the MWCNT support, followed by ultrasonication for inductively coupled plasma mass spectrometry (ICP-MS) (7500cx single-quad, Agilent Technologies) analysis. For every sample, a blank solution was prepared for ICP-MS analysis to account for an inherent copper content in the *aqua regia* solution that was not from the tested samples. A duplicate sample was prepared to ensure consistency of the results.

2.2.6. Copper dispersion and crystallite size

The CO chemisorption measurements were performed using BELCAT II Catalyst Analyzer (MicrotacBEL) (Fig. S1). Prior to measurement, the catalyst samples were first pretreated in the same unit. Approximately 0.05 g of the as-received commercial catalyst sample was pretreated by reduction in 5% H_2/95% Ar flowing at 50 sccm at 230 °C for 300 min. Another measurement was also conducted on a commercial catalyst that was reduced at 400 °C for comparison purposes. The as-prepared synthesized sample (0.03–0.05 g) was pretreated under He flowing at 50 sccm by heating from ambient temperature to 100 °C for 20 min, and the temperature was maintained at 100 °C for 15 min. The pretreatment condition employed was in compliant with the Catalysts Society of Japan. The same pretreatment procedure was followed for another measurement of the commercial catalyst without reduction with H_2. In some selected samples, the pretreatment temperature was varied to study the effect of the pretreatment temperature over a fixed duration, and the duration of the pretreatment temperature of 100 °C was varied to study the effect of the pretreatment duration at a constant temperature. After pretreatment, CO chemisorption by pulse injection was performed. For all catalyst samples, measurement was performed at 50 °C using CO as adsorption gas (10% CO/90% He flowing at 50 sccm) and stoichiometry factor of 1.0. He was used as the thermal conductivity detector (TCD) carrier gas flowing at 30 sccm in a low sensitivity TCD set at 100 °C. The adsorption gas was set to flow to the loop for 60 s, with the gas being injected to the sample cell in every 5 s. The measurement was repeated 2 times

to ensure reproducibility, assessing a sub-set of randomly selected samples.

2.3. Active site characterization study

Measurements were performed using BELCAT II Catalyst Analyzer on the same samples used previously for CO chemisorption. The CO adsorption was carried out by flowing 10% CO/90% He mixture at 50 sccm at 50 °C for 1 h, followed by a post-treatment in He flowing at 50 sccm at 50 °C for another hour. The CO-TPD measurement was then performed starting from 50 °C and heating to a target temperature of 400 °C at a ramping rate of 10 °C/min, in a target temperature holding time of 20 min. TCD was set at 100 °C and high sensitivity. The measurement was repeated 2 times to ensure reproducibility, assessing a sub-set of randomly selected samples. Hydrogen temperature programmed-reduction (H_2-TPR) was performed on the bare pristine and pre-functionalized MWCNTs by flowing 30 sccm of 5% H_2/95% Ar from 50 °C up to 600 °C at a ramping rate of 10 °C/min.

3. Results and discussion

3.1. Characterization

3.1.1. MWCNT support

Based on the certificate of analysis (COA) supplied by the vendor, the content of the carboxyl groups in the $MWCNT_{COOH}$ sample determined by X-ray photoelectron spectroscopy (XPS) analysis was 0.95–1.05%. The X-ray diffraction patterns of the pristine and $MWCNT_{COOH}$ were compared to ascertain the quality and crystallinity of these materials. In the diffraction patterns of the MWCNT samples, we focused on the peaks at 2θ = ~26.2 and ~42.5°, which correspond to the (0 0 2) and (1 0 0) reflections respectively (International Centre for Diffraction Data (ICDD) 01-075-1621). Peng & Liu (2006) [20] reported that the changes of the ratio of intensity of peak (1 0 0) to peak (0 0 2), I_{100}/I_{002} from the XRD patterns corresponded with the MWCNT's planar order, where a lower ratio of I_{100}/I_{002} indicates an increase in the degree of alignment to the (0 0 2) plane, which is the dominant facet of carbon. It was also found that the lower I_{100}/I_{002} ratio corresponds to an increase in the degree of crystallinity of the carbon ordering analysed using Raman spectroscopy. As seen from Fig. 1, when compared to the pristine MWCNT sample, the I_{100}/I_{002} ratio was significantly lower in the $MWCNT_{COOH}$ sample. This result supports a higher degree of crystallinity in the pre-functionalized $MWCNT_{COOH}$ sample.

TGA is used to estimate the relative degree of graphitization of MWCNT by measuring the decrease in mass of sample as a function of annealing temperature. Highly graphitized MWCNT generally decomposes at temperatures higher than that for carbon of lower ordering [21]. Unstable disordered carbon is combusted at temperatures below 500 °C, while the combustion of highly graphitized carbon takes place at temperatures above 600 °C [22,23]. From Fig. 2, it can be observed that the MWCNTs were, in general, thermally stable under nitrogen with a weight loss of 4.0% or below in the as-received pristine and pre-functionalized samples at 600 °C. At the end of the TGA test at 1200 °C, the pre-functionalized $MWCNT_{COOH}$ showed a weight loss of 11.3%, while the pristine MWCNTs showed a weight loss close to two times higher. This indicates the pristine MWCNTs contain some disordered carbon components that are unstable at very high temperatures.

Based on the zeta potential measurements, the negative surface charge of the pre-functionalized $MWCNT_{COOH}$ was –24.48 ± 1.46 mV, which was close to double the negative charge of the pristine MWCNTs; –15.43 ± 2.03 mV. This result is in alignment with the work published by Hamilton et al. (2013) [24], which demonstrated that a treatment with HNO_3 resulted in surface carboxylation of the carbon nanomaterials that made their surface charge more negative and helped suppress their hydrophobicity.

A brief dispersion/sedimentation test was conducted on the

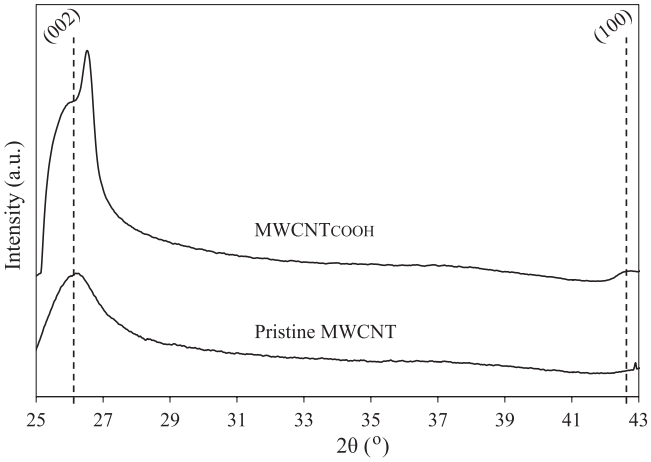

Fig. 1. XRD patterns of as-purchased pristine and pre-carboxyl-functionalized MWCNTs.

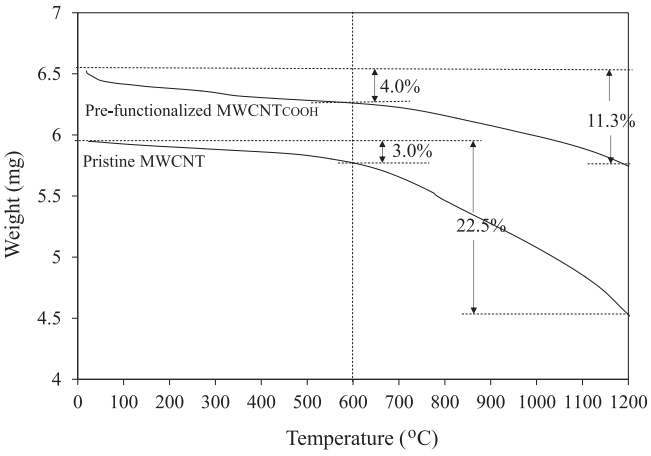

Fig. 2. TGA of as-purchased pristine and pre-carboxyl-functionalized MWCNTs.

MWCNT samples in DI water. Sedimentation of pristine MWCNTs was observed in DI water, even though the centrifugation parameters were halved in comparison to the pre-functionalized MWCNT samples. In contrast, the pre-functionalized $MWCNT_{COOH}$ was observed to disperse well in water, and the suspensions were found to be stable even after more than a week of storage (Fig. 3). This observation implies a satisfactory suppression of the hydrophobicity of the MWCNT surface in the $MWCNT_{COOH}$ sample.

3.1.2. Copper nanoclusters

The crystal structure was determined by single-crystal XRD (SCXRD) (Cambridge Crystallographic Data Centre (CCDC) # 1864974). The structure was solved in the monoclinic space group $P2_1$ with a = 14.28467 Å, b = 16.00824 Å, c = 21.39091 Å, α = 90°, β = 92.1229°, γ = 90°, Z = 2 and cell volume, V = 4888.16 Å^3. The structure has the empirical formula of $Cu_6P_6C_{111}H_{102}O_{0.75}$ due to 0.75 of a THF molecule being included in the structure. The complex of hexameric copper hydride ligated by triphenylphosphine, $[(PPh_3)CuH]_6$ (Fig. 4) can be compared to the hemisolvate structure, $[(PPh_3)CuH]_6$·0.5THF collected at room temperature by Albert et al. (1989) [18]. The differences in the unit cells (a = 14.464 Å, b = 16.252 Å, c = 21.487 Å) are likely due to the differences in temperature of the collection and loss of THF during the room temperature collection.

In the diffraction of the pure microcrystalline powder of Cu_6 nanocluster, the intensities of the experimental powder XRD (PXRD) pattern matched the predicted PXRD pattern generated from the SCXRD

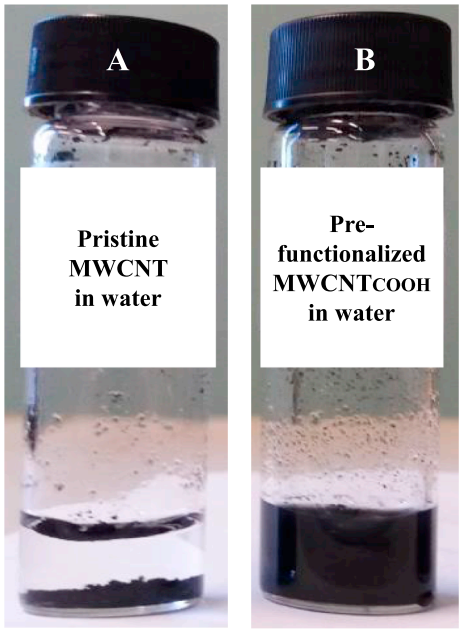

Fig. 3. (A) Sedimentation of pristine MWCNT in water; (B) well-dispersed $MWCNT_{COOH}$ in water after more than a week of storage.

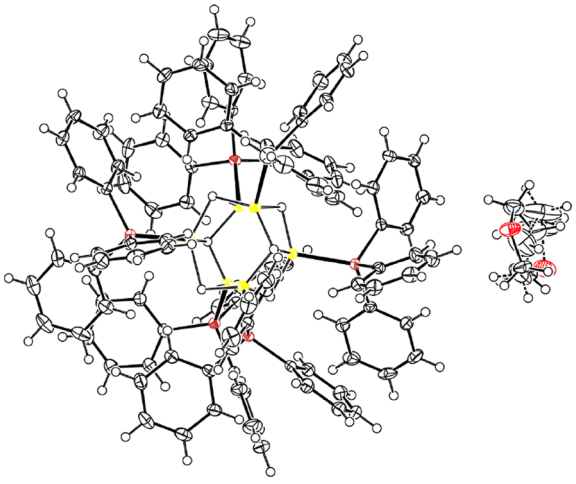

Fig. 4. Crystal structure complex of $[(PPh_3)CuH]_6{\cdot}0.75THF$ determined by SCXRD.

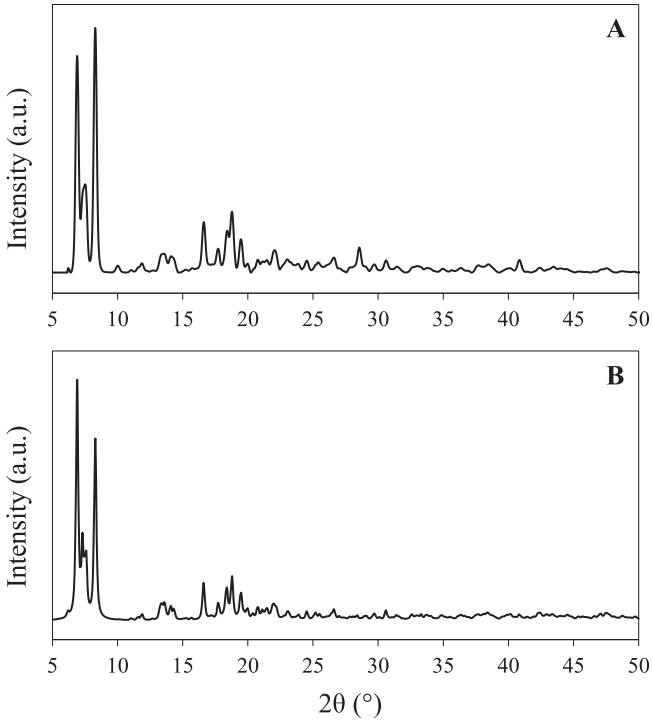

Fig. 5. PXRD patterns of Cu_6 nanocluster: (A) collected experimentally; and (B) generated from SCXRD (CCDC 1864974).

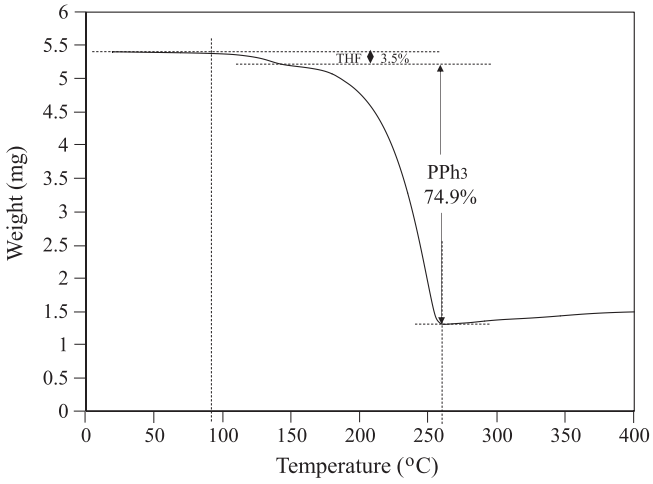

Fig. 6. TGA of $[(PPh_3)CuH]_6{\cdot}0.75THF$ nanoclusters.

result (Fig. 5), with a slight shift in the peak positions due to the experimental data being collected at two different temperatures (i.e. ambient temperature for PXRD and 120 K for SCXRD). The match in the intensities is better between the new structure (CCDC 1864974) than the previously reported one because the previous report [18] omitted the THF from the final refinement cycles. The experimental PXRD did not contain the powder patterns of other crystalline phases associated with copper crystallites; metallic Cu (ICDD 01-085-1326), oxide of Cu (I) (Cu_2O) (ICDD 01-077-0199), and oxide of Cu(II) (CuO) (ICDD 01-080-0076).

The TGA of the microcrystalline powder of the pure copper nanoclusters (Fig. 6) revealed that the nanoclusters lost approximately 78.4% of their original weight at 260 °C under nitrogen. The initial mass loss can be attributed to loss of THF solvate molecules (molecular weight (MW) = 72.11 g/mole) which desorbed first at a temperature below 100 °C (experimentally measured wt.% due to loss of THF – 3.5 wt%; calculated based on the empirical formula of $[(PPh_3)CuH]_6{\cdot}0.75THF$ (MW = 2,015.2 g/mole) – 2.7%). The next stage of sample decomposition can be explained by the loss of the PPh_3 ligand (MW = 262.29 × 6 mol = 1573.74 g/mole) in the temperature range from 150 to 260 °C, leaving behind the copper or copper hydride nanoparticles (experimentally measured wt.% loss due to loss of PPh_3 ligands – 74.9 wt%; calculated based on the empirical formula of $[(PPh_3)CuH]_6$ – 80.3%). It is impossible to reliably ascertain the fate of hydrides associated with Cu within cluster cores as such small mass loss (0.3% for all 6 of these) is within experimental error. The slight weight gain at the higher temperatures could indicate an onset of nitride or oxide formation, but this was not verified experimentally.

3.1.3. Catalysts

We used Cu_6 clusters to decorate MWCNTs and alumina supports with well-defined Cu active sites. However, we expect that prolonged exposure of the as-prepared samples to air would result in oxidation of clusters and formation of oxide nanoparticles even at room temperature

[2,25,26]. Yang et al. (2017) [26] synthesized size-selected Cu_n clusters on Al_2O_3 thin films and found that upon exposure of the samples to air, the as-deposited metallic Cu_n clusters underwent oxidation.

3.1.3.1. Copper content characterization. Based on ICP-MS data (Table 1), the experimentally measured copper loading in the Cu_6/$MWCNT_{COOH}$ catalyst sample was observed to be close to the calculated loading. The Cu species dispersion, surface area and crystallite size were calculated based on data obtained by using BELCAT II Catalyst Analyzer based on the amount of CO chemisorbed on 1.0 g of sample (Appendix A). The measurements by pulse CO chemisorption at 50 °C in general revealed an increasing copper crystallite size and reduced copper dispersion in the direction of the increasing copper loading content. The optimal copper loading content was identified to be 1 wt% based on the highest copper surface area per sample weight and the highest CO-adsorbed amount per sample weight at STP.

It is noted that the crystallite size of Cu species supported on alumina is more than double the size of its counterparts supported on MWCNTs, which could be explained by the huge difference in SSA of the three support materials, where the value is two orders of magnitude higher for MWCNTs than for alumina based on the product information provided by the vendors; 2.95 m^2/g for alumina, > 200 m^2/g (pristine MWCNTs), and > 100 m^2/g ($MWCNT_{COOH}$). The SSA of $MWCNT_{COOH}$ is half that of the pristine due to the carboxyl group occupancy of the sidewall surface of the MWCNTs. In addition, the dispersion of the Cu species is halved in alumina. This result indicates that the interaction between the Cu_6 nanoclusters and the alumina support is relatively less effective, resulting in a poorer dispersion.

The measurements were extended to observe the effect on copper sintering as a result of the catalyst pretreatment temperature increased and the heating duration prolonged. The results are presented in Table 2. In general, the copper crystallite size increases and the copper dispersion decreases in the direction of increasing pretreatment temperature at a fixed duration and with an increasing pretreatment duration at any given constant temperature.

Based on the measurements performed on 1%Cu_6/$MWCNT_{COOH}$, the results in Table 2 suggest a significant population of well-dispersed Cu species with high surface area was formed at 100 °C when heating was continued beyond 65 min. Surprisingly, when the sample was further heated for another 15 min, the copper nanoparticles sintered rather significantly, as evidenced by an increase in particle size, a reduction in the Cu surface area and diminution of the dispersion by close to 8 times.

The measurements on 1%Cu_6/$MWCNT_{COOH}$ were extended to pretreatment at 150 °C with an aim to determine the maximum temperature at which the sample could be pretreated before the effect of sintering started to appear while maintaining the duration of such treatment at 65 min. The 50 °C increase in treatment temperature resulted in 10-fold drop in the copper dispersion at 65 min. Similarly, a pretreatment at relatively low temperature of 100 °C for 80 min or pretreatment at relatively high temperature (400 °C) but only a short time (35 min) proved to be detrimental to the copper dispersion in a similar manner.

In general, at all the pretreatment conditions for activation of 1%Cu_6/$MWCNT_{COOH}$ even in the case of up to 400 °C for 35 min, this catalyst exhibited a significantly smaller Cu crystallite size and at least an order of magnitude higher dispersion than that of the commercial catalyst reduced at 230 °C (Table 1). The data for 13%Cu_6/$MWCNT_{COOH}$ up to 200 °C shows that even in the case of such high metal loading sample, the Cu crystallite size and dispersion are still better than that of commercial catalyst.

In our work, CO was used as the probe gas to study the chemisorption ability of the supported Cu_2O as the active phase for LTWGS. The formation of Cu_2O phase is presented next in this section. Although N_2O has been an established probe gas for Cu site measurement, the dispersion of Cu based on oxygen uptake by Cu(0) sites following the stoichiometry of dissociative N_2O adsorption ($N_2O + 2\ Cu \rightarrow$

Table 1
Cu crystallite size and dispersion.

Sample	Synthesis protocol	Sample condition	Calculated Cu content (wt.%)	Actual Cu content by ICP-MS (wt.%)	Cu particle diameter (nm)	Cu dispersion (%)	CO adsorbed amount per sample weight (cm^3/g (STP))	Cu surface area per sample weight (m^2/g)	Cu surface area per Cu weight (m^2/g)
Cu_6/$MWCNT_{COOH}$	• Copper (I) chloride + PPh_3 + K-selectride dissolved in THF prepared under Ar environment • Wet impregnation under Ar • No calcination	Heat-pretreated at 100 °C	0.5	0.64	2.5	41.9	0.95	1.73	269.99
			1	1.01	2.9 *(3.0)	35.6 *(35.4)	1.27 *(1.25)	2.31 *(2.28)	229.43 *(228.02)
			5	5.46	61.0	1.7	0.33	0.60	11.03
			11	11.69	66.4	1.6	0.65	1.18	10.13
			13	13.62	79.7	1.3	0.63	1.15	8.44
			15	15.02	111.7	0.9	0.50	0.91	6.02
Cu_6/Pristine MWCNT	• Same as above	Heat-pretreated at 100 °C	1		3.2 *(3.4)	32.4 *(31.1)	1.14 *(1.10)	2.09 *(2.01)	208.99 *(200.60)
Cu_6/Al_2O_3	• Same as above	Heat-pretreated at 100 °C	1		6.9	15.2	0.53	0.98	97.72
Cu_{NP}/$MWCNT_{COOH}$	• Copper (II) chloride dissolved in methanol prepared at ambient • Wet impregnation at ambient • Calcination in N_2 at 400 °C	Heat-pretreated at 100 °C	1		3.2	32.8	1.16	2.12	211.56
Commercial catalyst	• Confidential	Heat-pretreated at 100 °C	51		235.6	0.4	0.80	1.46	2.85
		Reduced at 230 °C	51		295.8	0.3	0.63	1.16	2.27
		Reduced at 400 °C	51		1188.2	0.1	0.16	0.29	0.57

* Experimentally reproduced data of selected samples.

Table 2
Effects of pretreatment temperature and duration.

Sample	Pretreatment temperature (°C)	Pretreatment duration (min)	Cu particle diameter (nm)	Cu dispersion (%)	Cu surface area per sample weight (m^2/g)	Cu surface area per Cu weight (m^2/g)
0.5%Cu_6/$MWCNT_{COOH}$	100	35	2.5	41.9	1.73	269.99
	400	35	20.4	5.1	0.21	32.96
1%Cu_6/$MWCNT_{COOH}$	100	35	2.9 *(3.0)	35.6 *(35.4)	2.31 *(2.28)	229.43 *(228.02)
	100	65	2.8	36.7	2.24	221.99
	100	80	23.0	4.5	0.30	29.29
	100	140	43.6	2.4	0.16	15.41
	150	65	28.5 *(32.8)	3.7 *(3.2)	0.24 *(0.21)	23.64 *(20.52)
	400	35	23.8	4.4	0.29	28.31
13%Cu_6/$MWCNT_{COOH}$	100	35	79.7	1.3	1.15	8.44
	200	35	90.9	1.1	1.01	7.40
	300	35	359.4	0.3	0.25	1.87
	400	35	596.0	0.2	0.15	1.13

* Experimentally reproduced data of selected samples.

$Cu_2O + N_2$) does not take into account the unreduced Cu^+ species [27]. The use of N_2O as the probe gas would not provide a well-represented measurement of the Cu(I) sites. This will have a different connotation since we are examining Cu_2O as the active Cu species for the LTWGS reaction in our study. In addition, whilst we can reduce the catalyst from Cu(I) to Cu(0) and then measure the Cu sites using N_2O, the following concerns are raised as the measurements are affected by variation in

i) The temperature and duration of Cu(I) reduction to Cu(0) (as evidenced by the findings presented in Table 2);
ii) the temperature of Cu(0) oxidation to Cu(I) by dissociative N_2O adsorption (N_2O reduction) [27].

Hua et al. (2013) [28] demonstrated the use of CO as the probe gas to measure the reducibility and chemisorption ability of Cu_2O nanocrystal facets of (1 0 0), (1 1 1) and (1 1 0) towards CO by CO-TPR and CO chemisorption and relate such measurements with the activity of the Cu_2O catalyst in the catalysis of CO oxidation. In their findings, different crystal planes exhibited different levels of activity in chemisorbing CO, which were shown to be consistent with their catalytic performance in CO oxidation. In general, this work validates the use of CO as the probe gas in the chemisorption on Cu_2O phase and, hence, provides good support for its employment in our study.

3.1.3.2. Phase composition. The PDFs of four prominent crystalline phases of copper; metallic Cu, CuH (Crystallography Open Database (COD) 96-900-8867), Cu_2O and CuO were used to analyse the as-prepared catalyst diffraction patterns (Fig. 7). Three peaks assigned to the dominant facets of Cu_2O crystal (1 1 1), (2 0 0) and (2 2 0) were positioned at $2\theta = 36.5$, 42.4 and 61.6° respectively. Cu_2O (2 0 0) overlapped with carbon plane (1 0 0) at $2\theta = \sim 42.2°$. The less dominant Cu_2O (1 1 0) peak could be more profoundly visualized at 29.6° only in higher Cu contents. The formation of Cu_2O in the catalyst samples even though the synthesis protocol did not include a calcination step in air or oxygen flow can be explained by the oxophilic nature of Cu, which is easily oxidized when in prolonged contact with air, even under ambient conditions [2,25,26].

The first-order significant Cu_2O peak ($2\theta = 36.5°$), which was the most dominant facet of the Cu_2O crystal phase, showed no distinguishable peak in the case of XRD of the sample containing 0.5% Cu_6. In the 1% Cu_6 sample, the diffraction pattern was almost identical to that of the 0.5% Cu_6 sample, with only a very small Cu_2O (1 1 1) peak appearing at 36.5°. This peak was more pronounced in the 5% Cu_6 catalyst sample, and its intensity increased further as the Cu_6 loading increased to 11% and 13%. However, the sample containing the 15% Cu_6 exhibited a peak of decreased intensity with a relative value between that of 11% and 5% Cu_6. In summary, the intensity of Cu_2O phase plane (1 1 1) increased with an increase in the Cu loading content, following the Cu_6 content in the order of $0.5\%Cu_6 \approx 1\%Cu_6 < 5\%Cu_6 < 15\%Cu_6 < 11\%Cu_6 < 13\%Cu_6$. The remaining dominant Cu_2O facets (2 0 0) and (2 2 0) showed peak intensity trends that were very (but not exactly) similar to Cu_2O (1 1 1).

Based on the results presented in Table 1, it is suggested that the surface area of Cu_2O crystallites is the factor that determines its catalytic activity. For instance, in the loading content order of $5\%Cu_6 < 15\%Cu_6 < 11\%Cu_6$, the Cu surface area in a gram of sample is $0.60 < 0.90 < 1.18\ m^2$, increasing in the same direction as the ratio of intensity of the Cu_2O (1 1 1) peak to intensity of any one of the MWCNT peaks. Although the Cu surface area was larger in the samples containing 0.5 and 1% Cu_6, their negligible intensity Cu_2O (1 1 1) peaks indicated a highly dispersed Cu(I) oxide structure phase on the $MWCNT_{COOH}$ support and a smaller crystallites size than the XRD lower detection limit of 4 nm [2,11]. These features are in agreement with the findings presented in Table 1. An XRD analysis was also performed on the sample of 0.5%Cu_6/$MWCNT_{COOH}$ that had undergone heat pretreatment at 100 °C. The results revealed an absence of the Cu_2O (1 1 1) peak position at 36.5° (Fig. S2), indicating that the crystallite size and dispersion of the Cu_2O phase on $MWCNT_{COOH}$ support were maintained.

The presence of copper oxide in the form of Cu_2O was further validated by H_2-TPR analysis of a representative catalyst sample, 1%Cu_6/$MWCNT_{COOH}$. During the reduction by 5% H_2 flowing in a nitrogen

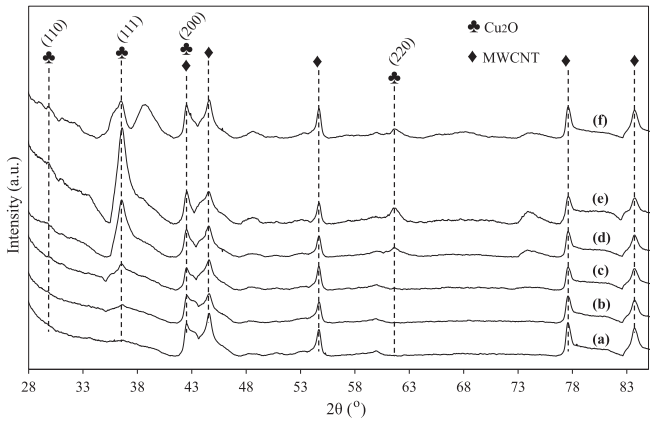

Fig. 7. XRD patterns of as-prepared Cu_6/$MWCNT_{COOH}$ catalysts of varied copper loading content of (a) 0.5%, (b) 1%, (c) 5%, (d) 11%, (e) 13%, and (f) 15%.

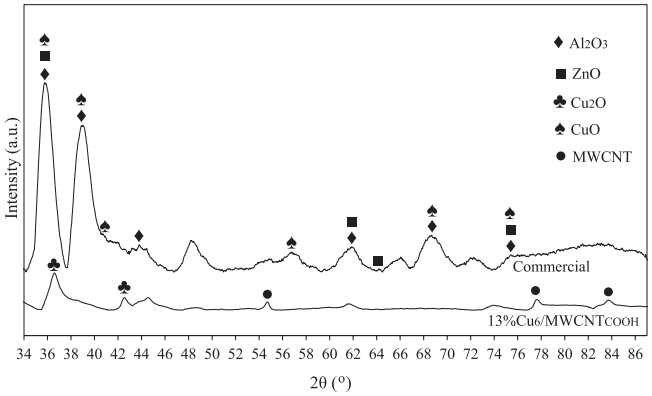

Fig. 8. XRD patterns of as-prepared 13%Cu_6/$MWCNT_{COOH}$ and as-received commercial catalyst samples.

carrier, the sample began to be reduced at approximately 300 °C up to slightly below 500 °C, as shown by the reduction peak (Fig. S3). The same reduction behaviour was exhibited by a powdered Cu_2O sample, as demonstrated by Kim et al. (2003) [29]. The alignment of these results confirmed the change in the CuH phase to Cu_2O once the Cu_6 nanoclusters had been impregnated on the $MWCNT_{COOH}$ support.

In a comparison between a representative Cu_6/$MWCNT_{COOH}$ catalyst (as-prepared) and the reference catalyst (as-received), the diffraction pattern of the 13%Cu_6/$MWCNT_{COOH}$ sample was used to represent the Cu_6/$MWCNT_{COOH}$ series due to its obvious appearance and significant intensity of the Cu_2O phase plane (1 1 1) at the peak position of 36.5°, as discussed earlier. Here we were objectively more interested in the crystalline phases associated with Cu, and therefore our attention was focused on the two oxides. As shown in Fig. 8, no peaks were detected at 2θ = 36.5 and 42.4° in the commercial catalyst, indicating the absence of the Cu_2O phase in the sample. The peaks that showed the characteristic of the CuO crystalline phase are clearly more profound in the commercial catalyst diffraction pattern at 2θ = 35.5 (–1 1 1), 38.6 (1 1 1), 39.0 (2 0 0), 56.6 (0 2 1), 68.8 (–2 2 1), and 74.9° (0 0 4). The peak attributed to the most dominant facet of CuO (–111) overlaps with ZnO (ICDD 01–075-1533) crystal plane (1 0 1) and Al_2O_3 (ICDD 01-075-0788) crystal plane (1 0 4) at 2θ = 35.5°, which is also observed on CuO (0 0 4) at 74.9°. The CuO phase planes (1 1 1) and (–2 2 1) overlap with alumina (1 1 0) and (3 0 0), respectively. The other remaining detected peaks confirm the presence of the CuO crystalline phase in the commercial catalyst sample. The presence of the CuO component in the commercial catalyst was further confirmed by H_2-TPR profile of its sample (Fig. S4), exhibiting a reduction curve beginning from approximately 200 °C under a mixture of 5% H_2/95% He, which is in alignment with the findings of Kim et al. (2003) [29].

The CuO phase was detected in the commercial catalyst sample as a result of its synthesis protocol, which typically involves calcination with oxygen/air to market the catalyst product to industry operators in a stable CuO form. The CuO peaks were not detected on the Cu_6/$MWCNT_{COOH}$ sample. The intensity of the peaks due to the Cu oxide species was more profound in the commercial catalyst due to the higher Cu loading content.

3.2. Active site characterization

Determination of the rate of reaction is possible by an estimation of the surface coverage and activation energy through a representation of the reaction using the microkinetic method, which is based on knowledge of the elementary steps involved in the reaction where the detailed chemistry of the reaction is explored. However, performing the microkinetic simulation by using the kinetics of the elementary steps is computationally intensive, although it can provide the accurate pathway and prediction of the reaction [7]. In this work, we combined the established knowledge on the elementary steps involved in LTWGS with an active site characterization technique using CO-TPD to hypothesize the activity of our synthesized Cu_6 nanoclusters supported on functionalized MWCNTs, as a first step towards qualifying its novelty to contribute to the existing literature.

We consider the associative mechanism, which is an adsorption–desorption model, as the basis of the kinetic model. The working principle of CO-TPD is also based on the adsorption and desorption of the CO species on active sites of the synthesized catalysts. In the associative mechanism, the interaction of the adsorbed CO and H_2O species forms an adsorbed intermediate that decomposes to H_2 and CO_2 [7]:

$$CO + H_2O \leftrightarrow \text{Intermediate} \leftrightarrow CO_2 + H_2 \quad (2)$$

Gokhale et al. (2008) [30] proposed a carboxyl-intermediate mechanism based on studies on Cu (1 1 1), the dominant facet of copper crystallites in commercial Cu-ZnO catalysts. It was also explained that the LTWGS reaction on these catalysts is structurally insensitive; therefore, the proposed mechanism and rate of reaction may be applied across different Cu facets. The carboxyl intermediate-associative mechanism for the forward LTWGS reaction on Cu (1 1 1), explained as a Langmuir-Hinshelwood (L-H) process given by Gokhale et al. (2008) [30], Callaghan et al. (2003) [31] and Fishtik and Datta (2002) [32], is used as the basis to hypothesize the activity of our newly developed catalysts:

$$CO + S \leftrightarrow CO\text{–}S \quad K_A = 1.5 \times 10^6 \quad E_a = 0 \quad (3)$$

$$H_2O + S \leftrightarrow H_2O\text{–}S \quad K_A = 1.0 \times 10^6 \quad E_a = 0 \quad (4)$$

$$H_2O\text{–}S + S \leftrightarrow OH\text{–}S + H\text{–}S \quad K_S = 1.0 \times 10^{13} \quad E_a = 25.4 \quad (5)$$

$$CO\text{–}S + OH\text{–}S \leftrightarrow COOH\text{–}S + S \quad K_S = 1.0 \times 10^{13} \quad E_a = 0 \quad (6)$$

$$COOH\text{–}S + S \leftrightarrow CO_2\text{–}S + H\text{–}S \quad K_S = 1.0 \times 10^{13} \quad E_a = 1.4 \quad (7)$$

$$COOH\text{–}S + OH\text{–}S \leftrightarrow CO_2\text{–}S + H_2O\text{–}S \quad K_S = 1.0 \times 10^{13} \quad E_a = 0.9 \quad (8)$$

$$CO_2\text{–}S \leftrightarrow CO_2 + S \quad K_D = 4.0 \times 10^{12} \quad E_a = 5.3 \quad (9)$$

$$H\text{–}S + H\text{–}S \leftrightarrow H_2\text{–}S + S \quad K_S = 1.0 \times 10^{13} \quad E_a = 15.3 \quad (10)$$

$$H_2\text{–}S \leftrightarrow H_2 + S \quad K_D = 6.0 \times 10^{12} \quad E_a = 5.5 \quad (11)$$

K_A, K_S, K_D = rate constants of the adsorption constant ($atm^{-1}.s^{-1}$), surface reaction (s^{-1}) and desorption ($atm^{-1}.s^{-1}$) respectively; E_a = heat of adsorption (kcal/mol).

The nature of the active sites of the Cu species (metallic or oxides) for the LTWGS reaction has remained vague [1]. Although a Cu metal surface has been established to provide the primary active site in the forward and the reverse shift [7,33], the LTWGS reaction can also be catalysed on both metallic and oxides of Cu [7]. The most recent article discussing the most active Cu facets for the LTWGS reaction has been published in *Nature Communications* by Zhang et al. (2017) [34]. In their work, they found that the activity and activation energy exhibited by Cu_2O nanocrystals when used directly in the LTWGS reaction were nearly identical to those of Cu nanocrystals. It was demonstrated by structural characterization that the Cu_2O nanocrystals underwent an *in situ* morphology-preserved reduction into Cu nanocrystals, whereby both Cu(0) and Cu(I) species co-existed on the Cu nanocrystals surfaces during the reaction up to 275 °C and were active in catalysing the LTWGS reaction. The typical operating temperature range practised industrially is 190–250 °C [1,10], and hence, the Cu_2O phase can also be active for the LTWGS reaction under industrial operating conditions.

As discussed earlier in our work, once deposited on the MWCNTs support, the hexameric copper hydride, $(CuH)_6$ changed its phase to Cu_2O by oxidation with air at ambient. Similar to the findings of Zhang et al. (2017) [34], the active facets of the Cu_2O precursor in our work were identified to be (1 1 0), (1 1 1), (2 0 0) and (2 2 0). Therefore, our synthesized catalysts should be readily active for the LTWGS reaction

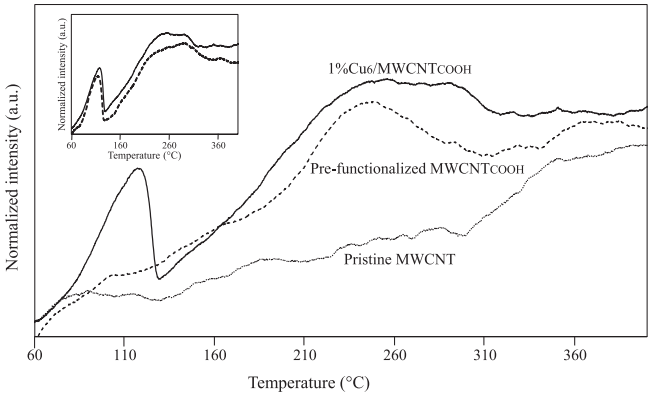

Fig. 9. CO-TPD profiles of 1%Cu_6/$MWCNT_{COOH}$ and pristine/pre-functionalized MWCNTs. Inset: reproduced CO-TPD profiles of 1%Cu_6/$MWCNT_{COOH}$.

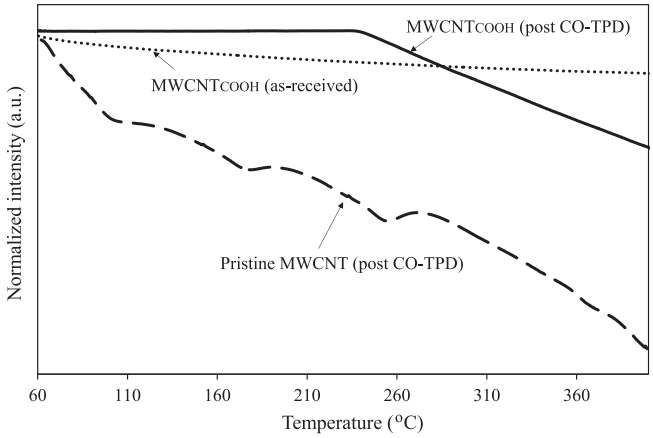

Figure 10

Fig. 10. H_2-TPR profiles of MWCNTs under various pretreatment conditions.

because they undergo an *in situ* morphology-preserved reduction as the reaction commences and progresses. As a result, an activation step by reduction with H_2 is not required. An activation protocol by ligand removal at a temperature above 260 °C through heat treatment under an inert flow may or may not be required for this newly developed catalyst, but this requirement must be experimentally determined prior to the activity test of the catalyst. Nevertheless, pretreatment at a low temperature of 100 °C is recommended to remove impurities that may be present in the as-prepared sample.

In Fig. 9, the CO-TPD profile of 1%Cu_6/$MWCNT_{COOH}$ showed a small shoulder, low peak at 120 °C, and a broader, higher peak at approximately 245 °C. The desorption-peak at the lower temperature is identified as the active site on Cu_2O planes for the LTWGS reaction to occur. The appearance of this peak indicates the presence of an active site on the Cu_2O surface that interacts with the CO species and, hence, validates the hypothesis that the catalyst is readily active for the reaction to occur.

The narrow-shouldered peak at the lower temperature indicates a weak interaction between CO and the active site. The area under the peak profile is proportional to the surface coverage, which is the amount of CO originally adsorbed [35]. Its low peak maximum suggests a low surface coverage of CO (Eq. (3)), which should be meaningful for the reaction, as the remaining surface of the active site should be reserved for the H_2O molecule to occupy (Eq. (4)) to allow the remaining elementary steps (Eqs. (5)–(11)) to subsequently occur for CO conversion to H_2 and CO_2.

The peak maximum position along the desorption temperature axis is related to the desorption activation energy. As adsorption is a spontaneous process, the heat of adsorption therefore equals the activation energy for desorption [35]. The CO adsorption enthalpy given in Eq. (3), E_a = 0 kcal/mol, is nil or extremely low. Therefore, the peak position at the low temperature (120 °C) could well be attributed to elementary step (3). This result hypothetically suggests that 1%Cu_6/$MWCNT_{COOH}$ could be kinetically very active at temperatures as low as 120 °C. Based on the operating manuals by various catalyst manufacturers, the bed inlet temperature should be at least 20 °C above the water dew point at a particular operating pressure at all times, to avoid water condensation either in the catalyst pores or onto the bed, which would deactivate the catalyst. Note that 120 °C is the lowest temperature at which the LTWGS reaction can be operated due to water dew point limitation at atmospheric pressure, which is the pressure used in the TPD/R measurements in this work.

The second peak on the CO-TPD profile of 1%Cu_6/$MWCNT_{COOH}$ at the higher peak maximum temperature position of 245 °C is assigned the active site attributed to the surface oxygen (–COOH) grafted on the pre-functionalized MWCNTs. This peak was present in the profile of bare pre-functionalized $MWCNT_{COOH}$, but absent in that of bare pristine MWCNTs. The broader shoulder and higher peak maximum at higher temperature of the peak indicates a stronger CO interaction and more CO surface coverage on this active site, which is not useful for the LTWGS reaction due to its high activation energy for CO desorption. The CO desorption becomes more difficult because of the need to overcome the higher energy obstacle.

Nevertheless, the peak attributed to the oxygen-moiety groups at 245 °C could hypothetically provide an active site that could have broken the chemical bond between the carboxyl groups grafted on the surface of the functionalized MWCNTs and carbon, causing the carboxyl groups to become unstable and, hence, decompose into O_2 and H_2. This process was then followed by CO oxidation to produce CO_2 in the CO-TPD. Performing a hydrogen temperature-programmed reduction (H_2-TPR) on bare $MWCNT_{COOH}$ would help explain this possibility. H_2-TPR up to 600 °C was performed on the bare pristine and pre-functionalized MWCNTs to determine the temperature at which the oxygen-moiety (carboxyl) groups create an active site for CO adsorption or are possibly reactive in the reaction environment. A close-up of the intensity of the H_2-TPR spectrum of bare $MWCNT_{COOH}$ (Fig. 10) showed that the as-received sample exhibited a straight line. In contrast, the H_2-TPR profile of the bare $MWCNT_{COOH}$ sample that had undergone CO-TPD up to 400 °C prior to the H_2-TPR measurement exhibited an altered behaviour, where the straight intensity line was followed by a drop in the TCD signal, providing a declination slope from a temperature point of approximately 240 °C. This phenomenon did not occur in the post-CO-TPD pristine MWCNT sample.

It is suggested that the oxygen groups were removed from the vacant sites that had been previously occupied (adsorbed) by CO, at 240 °C and beyond. In the LTWGS reaction environment, the chemical bond binding the carboxyl groups and the carbon would break at 240 °C, resulting in a decomposition of the carboxyl groups. In this H_2-TPR measurement, the decomposed carboxyl was subsequently swept out of the system by H_2, as indicated by the drop in the TCD signal. H_2 did not react with (reduce) the decomposed oxygen-groups gases, which would have otherwise been signalled as a reduction peak in the H_2-TPR profile.

It is speculated that from 240 °C, the loss of the oxygen groups from the MWCNT surface deteriorates the dispersion of the Cu_2O phase. This phenomenon is supported by the results shown in Table 2, where the dispersion significantly deteriorated when the representative sample, 13%Cu_6/$MWCNT_{COOH}$, was heated at 300 °C (dispersion, d = 0.29%) in comparison to that at 200 °C (d = 1.15%), which was comparable to that at 100 °C (d = 1.31%). However, we cannot deny the possibility that the poor dispersion post-heating at 300 °C could also have been caused by sintering of the Cu species itself. Cu is susceptible to thermal sintering at temperatures beyond 300 °C [7]. Again, this is evident by the results shown in Table 2, where the crystallite size of the Cu species

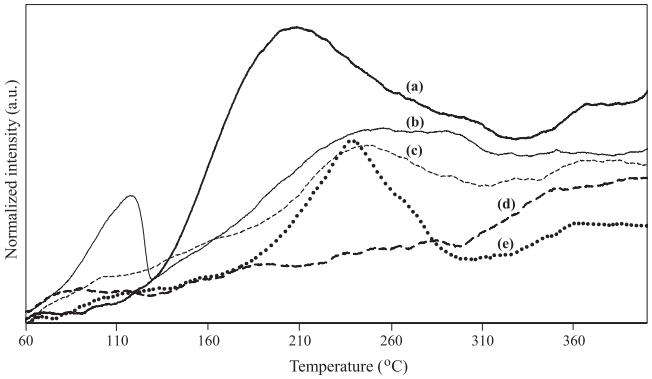

Fig. 11. CO-TPD profiles of (a) 1%Cu_6/pristine MWCNT, (b) 1%Cu_6/MWCNT$_{COOH}$, (c) bare pre-functionalized MWCNT$_{COOH}$, (d) bare pristine MWCNT, and (e) 1%Cu_{NP}/MWCNT$_{COOH}$.

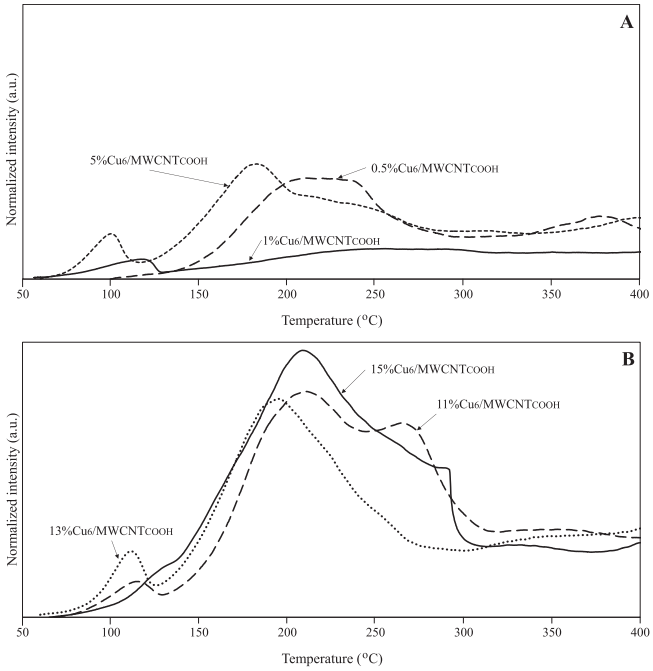

Fig. 12. CO-TPD profiles of Cu_6/MWCNT$_{COOH}$ catalysts of varied Cu content: (A) 0.5, 1 and 5%; and (B) 11, 13 and 15%.

became significantly larger after undergoing heat treatment at 300 °C in comparison to those at 200 and 100 °C, which were reasonably comparable to each other.

Therefore, the maximum operating temperature for 1%Cu_6/MWCNT$_{COOH}$ should be capped at below 190 °C, allowing room for the temperature rise associated with the reaction exotherm. This guidance is vital, especially in current industrial practices in existing plants that are designed to typically operate the LTWGS reaction in a range from 190 to 250 °C [1,10] at a typical operating pressure ranging from 25 to 35 bar [5]. The lower limit of the operating temperatures in which the LTWGS reaction is run under industrial conditions is 190 °C at a typical operating pressure of 30 bar, which is imposed by the water dew point [7,10].

In the CO-TPD profile of the corresponding 1%Cu_6 catalyst sample supported on pristine MWCNTs (Fig. 11), the peak-maximum position of the first peak, which was attributed to the Cu_2O active site, shifted to 210 °C and became broader and higher, resulting in a larger area under the profile. Without the presence of the carboxyl groups, the active site for the LTWGS reaction exhibited a stronger interaction with more surface coverage of CO species, causing CO desorption to become more difficult due to its higher activation energy and concentration. This finding indicates a kinetically less active catalyst exhibited by 1%Cu_6/pristine MWCNT as elementary steps (3) and (6) have a higher energy obstacle to overcome.

In the case of the corresponding catalyst consisting of Cu nanoparticles supported on MWCNT$_{COOH}$ (1%Cu_{NP}/MWCNT$_{COOH}$), only one profound peak was observed within the temperature range up to 400 °C. This peak was assigned to the Cu_2O active site. The peak attributed to the carboxyl groups had collapsed, where the oxygen groups should have been removed from the as-prepared sample at the calcination stage that took place at 400 °C, which was part of the synthesis protocol. The peak-maximum position was at approximately 240 °C, indicating a kinetically less active catalyst in comparison to its Cu_6 nanocluster counterpart (1%Cu_6/MWCNT$_{COOH}$). In contrast, the lower peak and narrower shoulder of 1%Cu_{NP}/MWCNT$_{COOH}$ in comparison to that of 1%Cu_6/pristine MWCNT indicated a lower CO surface coverage on the active site, which could hypothetically be translated into the possibility of a higher CO conversion performance as the less concentrated surface coverage by the adsorbed CO species (Eq. (3)) provided availability for H_2O adsorption (Eq. (4)) and allowed the subsequent elementary steps to occur.

Fig. 12 shows the different behaviours of the Cu_6/MWCNT$_{COOH}$ catalyst when loaded with various loading contents. At 0.5 wt% loading, the first peak, which is assigned to Cu_2O active site, appeared broader and higher and was shifted to the right. The peak attributed to the carboxyl group had collapsed above 240 °C, but a new, stronger peak appeared at 375 °C, which can be assigned to another active site of Cu_2O but is not useful in the LTWGS reaction as it exceeded the operating temperature limit of 300 °C at which the sintering of Cu occurs. The 5% Cu loading content exhibited similar behaviour to that of the 1%, but the position of the peak-maximum of the Cu_2O active site occurred at a temperature that is low for the LTWGS reaction, which is slightly below the dew point of water.

The catalysts containing 11% and 13% Cu exhibited a similar profile in their first peak associated with Cu_2O, but their second peak attributed to the carboxyl groups was shifted to 210 and 195 °C, respectively. Hypothetically, this could result in catalyst deactivation at operating temperatures lower than that for the 1%Cu_6/MWCNT$_{COOH}$ catalyst. The third peak in the profile of the 11%Cu_6/MWCNT$_{COOH}$ catalyst at approximately 270 °C could be assigned to decarboxylation or the Cu_2O active sites, but it is not meaningful for LTWGS reaction operating temperatures, which are typically capped at 250 °C to avoid Cu sintering.

The 15%Cu_6/MWCNT$_{COOH}$ catalyst is predicted to lack meaningful kinetic activity for the LTWGS reaction because its Cu_2O peak is almost negligible at the peak-maximum position of 130 °C and overlaps with the broad peak profile belonging to the carboxyl groups.

CuO-ZnO catalysts require activation by exposure to a dilute H_2 flow in the process stream to reduce the Cu(II) directly to Cu(0), following an exothermic reaction (Eq. (12)) at 230 °C [7,29,36]:

$$CuO\ (s) + H_2\ (g) \rightarrow Cu\ (s) + H_2O\ (g) \quad \Delta H = -80.8\ kJ/mol \qquad (12)$$

From the results shown in Table 1, the crystallite size of the Cu species was substantially larger in the commercial catalyst sample that was reduced at 400 °C, while the Cu size was comparable between the unreduced catalyst and the catalyst that was reduced at 230 °C. Fig. 13 shows the CO-TPD profiles of the as-prepared 1%Cu_6/MWCNT$_{COOH}$ and 1%Cu_6/Al_2O_3 catalysts and activated commercial catalyst, reduced at 230 and 400 °C. The two active site peaks observed on the commercial catalyst reduced at 230 °C collapsed in the profile of the one that was reduced at 400 °C, exhibiting an almost negligible active site peak similar to the profile of the inert alumina. It is evident that the Cu particles underwent sintering because of surface migration after heat exposure above 300 °C, which led to catalyst deactivation [5,7,31].

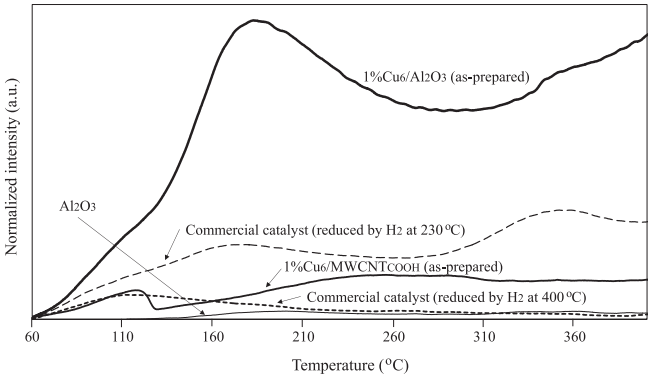

Fig. 13. CO-TPD profiles of as-prepared 1%Cu_6 supported on $MWCNT_{COOH}$ and alumina and the reduced commercial catalyst.

At lower reaction temperatures than the industrial LTWGS reaction operating temperatures (i.e., < 190 °C), the 1%Cu_6/$MWCNT_{COOH}$ catalyst is expected be more active kinetically than the commercial catalyst (reduced to Cu(0) at 230 °C) based on the observed predominant peak (between 110 °C and 210 °C) in the CO-TPD profiles attributed to the active sites of the Cu species. However, as discussed earlier, the operating temperature of the 1%Cu_6/$MWCNT_{COOH}$ catalyst has an upper limit and should be capped at below the typical LTWGS operating temperatures to avoid deactivation by Cu sintering. In an actual activity test performed under typical industrial LTWGS operating conditions (reaction temperature = 190–250 °C, GHSV = 2,750–8,650 h^{-1}), CO conversion over 1%Cu_6/$MWCNT_{COOH}$ was found to be < 1.0%, indicating an effect of deactivation, while the reference catalyst exhibited a conversion of 84.2–93.8%. This actual activity test result validates our prediction by CO-TPD that the 1%Cu_6/$MWCNT_{COOH}$ is deactivated when operated under industrial operating conditions. The second peak in the profile of the commercial catalyst is not useful for LTWGS operating conditions. The corresponding Cu_6 catalyst supported on alumina exhibited a Cu_2O active site peak that is much broader and of higher intensity in comparison to peak observed in the case of an activated commercial catalyst and is therefore speculated to have poor kinetic activity in the LTWGS reaction.

4. Conclusions

A prediction of catalytic activity and/or deactivation of catalyst in the LTWGS reaction based on surface chemistry and structural characterization by XRD and CO chemisorption and active site characterization by CO-TPD have been demonstrated on a newly developed, potentially novel catalyst consisting of hexameric copper hydride nanoclusters ligated to PPh_3, solvated with THF, supported on functionalized MWCNTs, and synthesized by the wet impregnation method without undergoing a calcination post-impregnation.

The hexameric copper hydride nanoclusters changed their phase to a highly dispersed Cu_2O phase with oxidation in air under ambient conditions when the complex had been deposited onto the surface of the functionalized MWCNTs. The Cu_2O crystal planes (1 1 0), (1 1 1), (2 0 0) and (2 2 0) were found to be the active facets for CO reactivity based on XRD characterization. Since Cu_2O phases are readily active for LTWGS to occur, an activation protocol by reduction with H_2 or by ligand removal at a temperature above 260 °C through heat treatment under an inert flow may not be required. However, pretreatment at a low temperature of 100 °C is recommended to remove impurities that may be present in the as-prepared sample.

The employed CO-TPD technique serves as a first round screening of catalyst activity evaluation, while in parallel provides a means for effective planning in the selection of the operating conditions for the reaction run test because it supplies an indication of the operating conditions in which the catalyst activity may be at its highest potential, and the possible conditions in which deactivation might occur. Hence, an optimal operating condition for a maximum CO conversion allowed by thermodynamics in the equilibrium-limited LTWGS reaction could hypothetically be determined.

It is expected that the optimal catalyst, 1%Cu_6/$MWCNT_{COOH}$, should be active for the LTWGS reaction within a range of lower temperatures compared to the industrial LTWGS reaction operating temperatures. In the case of other catalysts, their feasible operating temperature range will change with the loading of the active Cu species. In general, the lower operating temperature limit is imposed by the water dew point, while the upper limit is constrained by the temperature rise from the reaction exotherm that could lead to Cu sintering. Depending on the Cu_6 content in the catalyst, extra care must be taken when running the exothermic LTWGS reaction over the catalyst to avoid irreversible Cu sintering due to the removal of carboxyl groups, which has been experimentally validated.

Acknowledgements

The authors acknowledge the financial support of the Department of Chemical and Process Engineering (CAPE), University of Canterbury (UC), Christchurch, New Zealand. The authors would like to thank Felicitas Jansen of Rheinisch-Westfälische Technische Hochschule Aachen, Germany for performing the copper nanocluster's TGA and SCXRD experiments; Robert Stainthorpe, Technician of School of Physical and Chemical Sciences, UC for ICP-MS analysis; and Wasim Ullah Khan, CAPE PhD candidate for his help in performing some of the CO-TPD and H2-TPR analyses.

Appendix A. Supplementary data

Supplementary data to this article can be found online at https://doi.org/10.1016/j.cej.2018.10.215.

References

[1] D. Mendes, et al., Determination of the low-temperature water–gas shift reaction kinetics using a Cu-based catalyst, Ind. Eng. Chem. Res. 49 (22) (2010) 11269–11279.
[2] N.M. Oliveira, G.P. Valençaa, R. Vieirab, Water gas shift reaction on copper catalysts supported on alumina and carbon nanofibers, Chem. Eng. 43 (2015).
[3] A. Luengnaruemitchai, S. Osuwan, E. Gulari, Comparative studies of low-temperature water–gas shift reaction over Pt/CeO2, Au/CeO2, and Au/Fe2O3 catalysts, Catal. Commun. 4 (5) (2003) 215–221.
[4] E. Demirel, N. Azcan. Thermodynamic modeling of water-gas shift reaction in supercritical water, in: Proceedings of the World Congress on Engineering and Computer Science, 2012.
[5] N. Schumacher, et al., Trends in low-temperature water–gas shift reactivity on transition metals, J. Catal. 229 (2) (2005) 265–275.
[6] Y. Li, Q. Fu, M. Flytzani-Stephanopoulos, Low-temperature water-gas shift reaction over Cu-and Ni-loaded cerium oxide catalysts, Appl. Catal. B 27 (3) (2000) 179–191.
[7] B.S. Rj, M. Loganathan, M.S. Shantha, A review of the water gas shift reaction kinetics, Int. J. Chem. Reactor Eng. (2010) 8.
[8] L. Baharudin, M.J. Watson, Hydrogen applications and research activities in its production routes through catalytic hydrocarbon conversion, Rev. Chem. Eng. 34 (1) (2017) 43–72.
[9] R. Smith, M. Loganathan, M.S. Shantha, A review of the water gas shift reaction kinetics, Int. J. Chem. Reactor Eng. (2010) 8(1).
[10] C. Ratnasamy, J.P. Wagner, Water gas shift catalysis, Catal. Rev. 51 (3) (2009) 325–440.
[11] T. Maniecki, P. Mierczyński, W. Jóźwiak, Copper-supported catalysts in methanol synthesis and water gas shift reaction, Kinet. Catal. 51 (6) (2010) 843–848.
[12] G.C. Chinchen, et al., Promotion of methanol synthesis and the water-gas shift reactions by adsorbed oxygen on supported copper catalysts, J. Chem. Soc., Faraday Trans. 1 F 83 (7) (1987) 2193–2212.
[13] S. Morales-Torres, et al., Palladium and platinum catalysts supported on carbon nanofiber coated monoliths for low-temperature combustion of BTX, Appl. Catal. B 89 (3–4) (2009) 411–419.
[14] N.A. Jarrah, et al., Immobilization of a layer of carbon nanofibres (CNFs) on Ni foam: a new structured catalyst support, J. Mater. Chem. 15 (19) (2005) 1946–1953.
[15] J.K. Chinthaginjala, L. Lefferts, Influence of hydrogen on the formation of a thin layer of carbon nanofibers on Ni foam, Carbon 47 (14) (2009) 3175–3183.
[16] J.K. Chinthaginjala, et al., How carbon-nano-fibers attach to Ni foam, Carbon 46

(13) (2008) 1638–1647.
[17] L. Baharudin, et al., Potential of metal monoliths with grown carbon nanomaterials as catalyst support in intensified steam reformer: a perspective, Rev. Chem. Eng. (2018), https://doi.org/10.1515/revce-2018-0007 ahead of print.
[18] C.F. Albert, et al., Lewis-base adducts of Group 11 metal (I) compounds. 49. Structural characterization of hexameric and pentameric (triphenylphosphine) copper (I) hydrides, Inorg. Chem. 28 (7) (1989) 1300–1306.
[19] A.W. Cook, et al., Synthesis, Characterization, and Reactivity of the Group 11 Hydrido Clusters [Ag6H4 (dppm) 4 (OAc) 2] and [Cu3H (dppm) 3 (OAc) 2], Inorg. Chem. (2016).
[20] Y. Peng, H. Liu, Effects of oxidation by hydrogen peroxide on the structures of multiwalled carbon nanotubes, Ind. Eng. Chem. Res. 45 (19) (2006) 6483–6488.
[21] K.A. Wepasnick, et al., Chemical and structural characterization of carbon nanotube surfaces, Anal. Bioanal. Chem. 396 (3) (2010) 1003–1014.
[22] V. Datsyuk, et al., Chemical oxidation of multiwalled carbon nanotubes, Carbon 46 (6) (2008) 833–840.
[23] R.A. Moraes, et al., The effect of different chemical treatments on the structure and stability of aqueous dispersion of iron-and iron oxide-filled multi-walled carbon nanotubes, J. Braz. Chem. Soc. 22 (11) (2011) 2191–2201.
[24] R.F. Hamilton Jr.et al., Purification and sidewall functionalization of multiwalled carbon nanotubes and resulting bioactivity in two macrophage models, Inhalation Toxicol. 25 (4) (2013) 199–210.
[25] H.-M. Yang, P.-H. Liao, Preparation and activity of Cu/ZnO-CNTs nano-catalyst on steam reforming of methanol, Appl. Catal. A 317 (2) (2007) 226–233.
[26] B. Yang, et al., Copper cluster size effect in methanol synthesis from CO2, J. Phys. Chem. C 121 (19) (2017) 10406–10412.
[27] A. Dandekar, R. Baker, M. Vannice, Carbon-supported copper catalysts: I. Characterization, J. Catal. 183 (1) (1999) 131–154.
[28] Q. Hua, et al., Crystal-plane-controlled surface chemistry and catalytic performance of surfactant-free Cu2O nanocrystals, ChemSusChem 6 (10) (2013) 1966–1972.
[29] J.Y. Kim, et al., Reduction of CuO and Cu2O with H2: H embedding and kinetic effects in the formation of suboxides, J. Am. Chem. Soc. 125 (35) (2003) 10684–10692.
[30] A.A. Gokhale, J.A. Dumesic, M. Mavrikakis, On the mechanism of low-temperature water gas shift reaction on copper, J. Am. Chem. Soc. 130 (4) (2008) 1402–1414.
[31] C. Callaghan, et al., An improved microkinetic model for the water gas shift reaction on copper, Surf. Sci. 541 (1–3) (2003) 21–30.
[32] I. Fishtik, R. Datta, A UBI–QEP microkinetic model for the water–gas shift reaction on Cu (1 1 1), Surf. Sci. 512 (3) (2002) 229–254.
[33] C.Á. Galván, et al., Reverse water-gas shift reaction at the Cu/ZnO interface: influence of the Cu/Zn ratio on structure-activity correlations, Appl. Catal. B 195 (2016) 104–111.
[34] Z. Zhang, et al., The most active Cu facet for low-temperature water gas shift reaction, Nat. Commun. 8 (1) (2017) 488.
[35] V. Rakić, L. Damjanović, Temperature-Programmed Desorption (TPD) methods, in calorimetry and thermal methods, Catalysis (2013) 131–174 Springer.
[36] C. Rhodes, G.J. Hutchings, Studies of the role of the copper promoter in the iron oxide/chromia high temperature water gas shift catalyst, PCCP 5 (12) (2003) 2719–2723.